

Supporting Information

Long-Life Superlithiation of Few-Layered Covalent Organic Nanosheets *via* Graphene Quantum Dots/Carbon Nanotubes Stabilized Three-Dimensional Architecture

Xiudong Chen,^{a,b,†} Chenggang Ci,^{c,†} Weiwei Sun,^{a,†} Shuangqiang Chen,^a Hao Liu,^a and Yong Wang^{a,*}

^a Department of Chemical Engineering, School of Environmental and Chemical Engineering, Shanghai University, 99 Shangda Road, Shanghai, P. R. China, 200444

^b School of Chemistry and Chemical Engineering, Jiangxi Province Engineering Research Center of Ecological Chemical Industry, Jiujiang University, Jiujiang, Jiangxi, P. R. China, 332005

^c School of Chemistry and Chemical Engineering, Qiannan Normal College for Nationalities, Duyun, Guizhou, P. R. China, 558000

E-mail: yongwang@shu.edu.cn

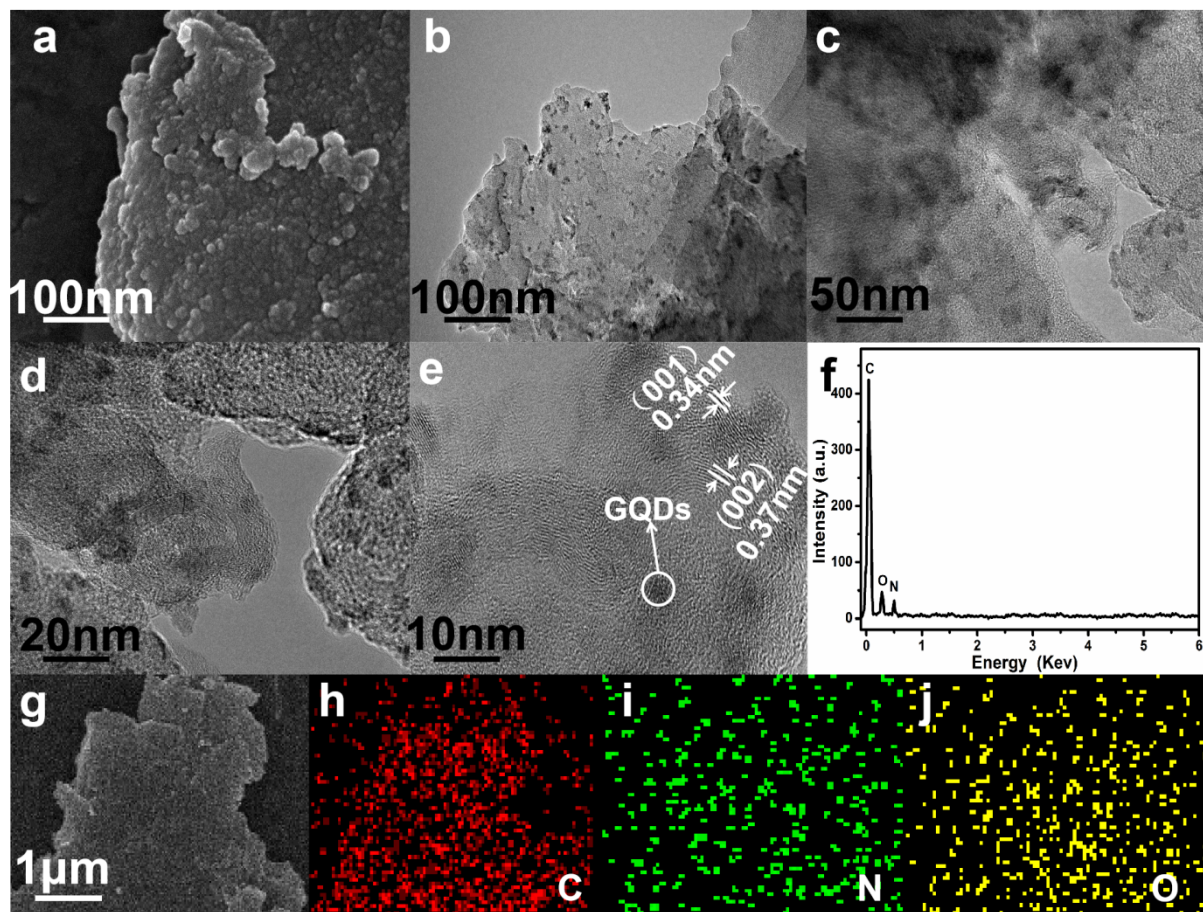


Fig. S1 Morphology characterizations of E-CONs/GQDs. a) SEM image, b) TEM image, c-e) HRTEM images, f) the EDS pattern, g-j) elemental mapping images.

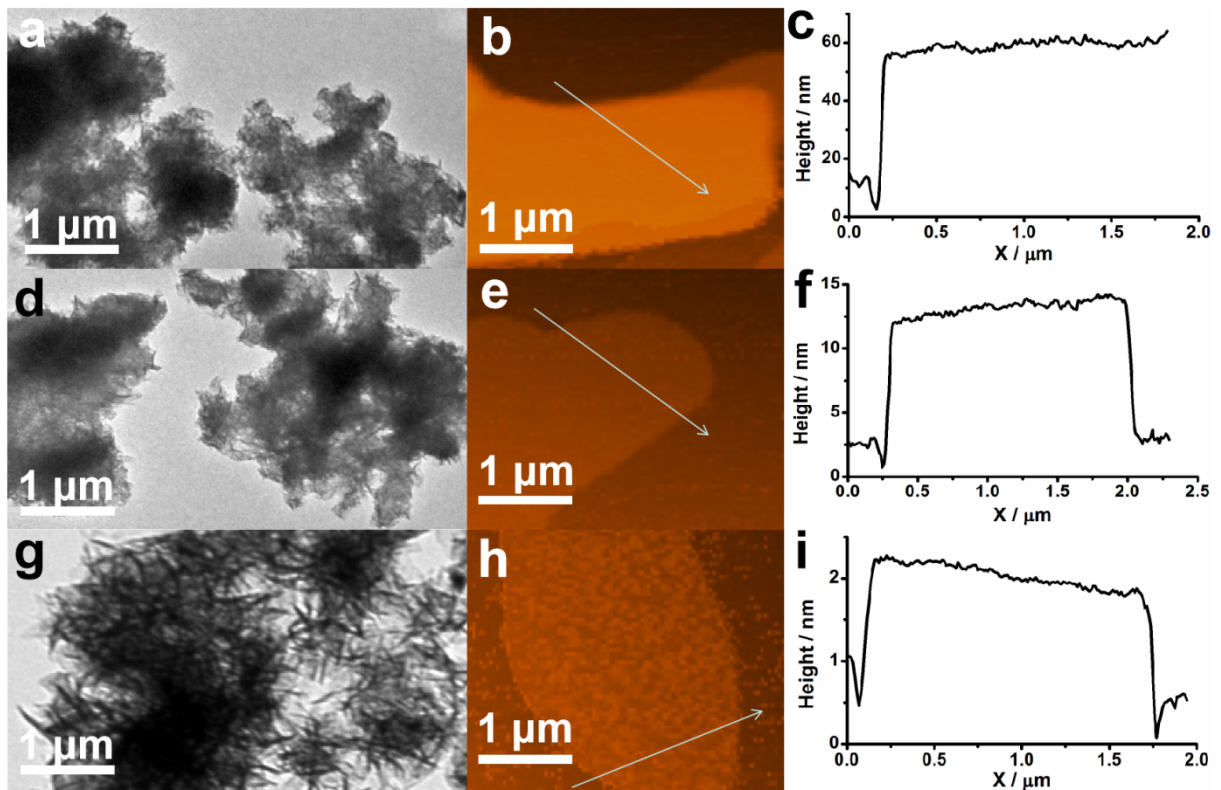


Fig. S2. Morphologies of the control samples. a) TEM image of E-CONs/GQDs-2H, (b) AFM image and (c) the measured thickness of E-CONs/GQDs-2H nanosheets. (d) TEM image of E-CONs/GQDs-4H, (e) AFM image and (f) the measured thickness of E-CONs/GQDs-4H nanosheets. (g) TEM image of E-CONs/GQDs-10H, (h) AFM image and (i) the measured thickness of E-CONs/GQDs-10H nanosheets.

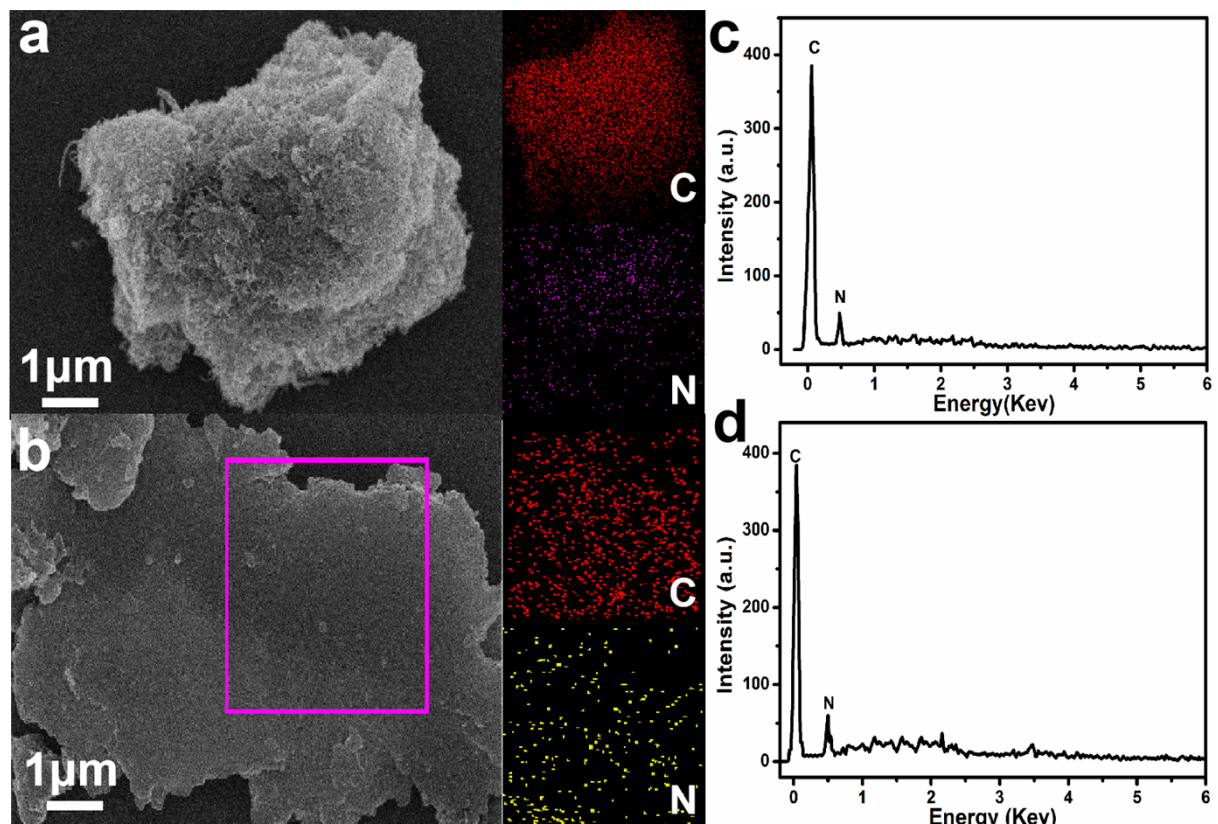


Fig. S3 Elemental mapping images and EDS pattern of CON and E-CONs. Elemental mapping images of a) CON and b) E-CONs. EDS pattern of c) CON and d) E-CONs.

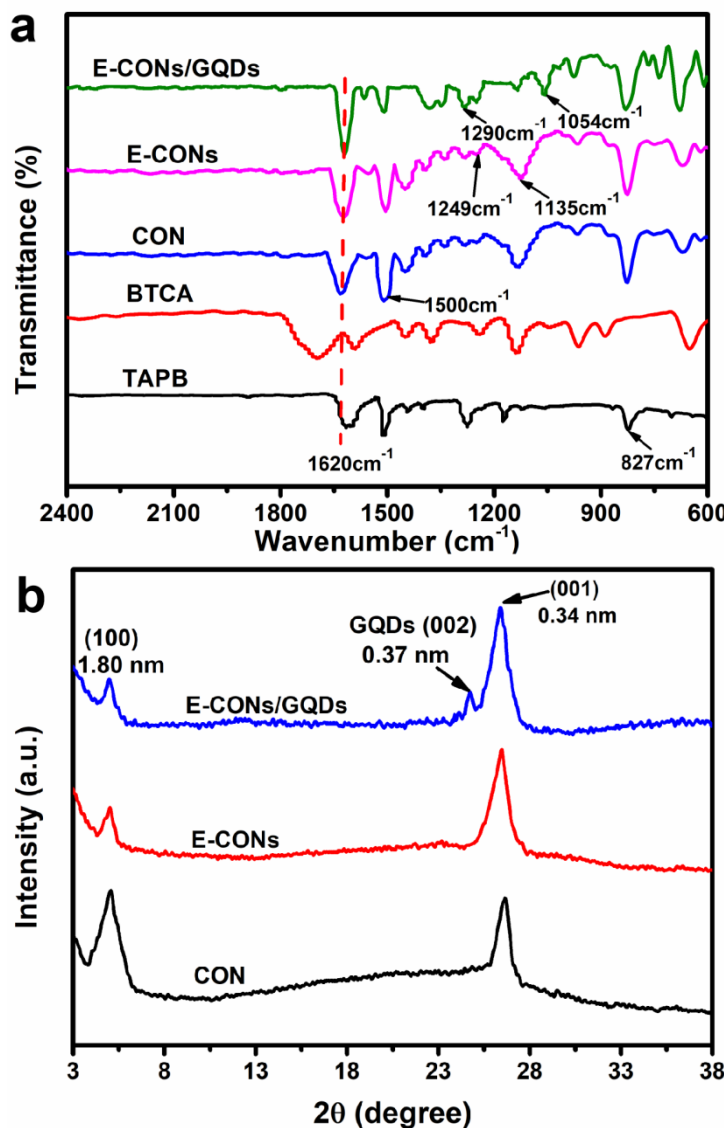


Fig. S4 Characterizations of E-CONs/GQDs and the control samples. a) FTIR spectra of the 1,3,5-tris(4-aminophenyl)benzene (TAPB), 1,3,5-benzenetricarbaldehyde (BTCA), E-CONs, E-CONs/GQDs, and CON. b) Powder XRD patterns of E-CONs/GQDs, E-CONs, and CON.

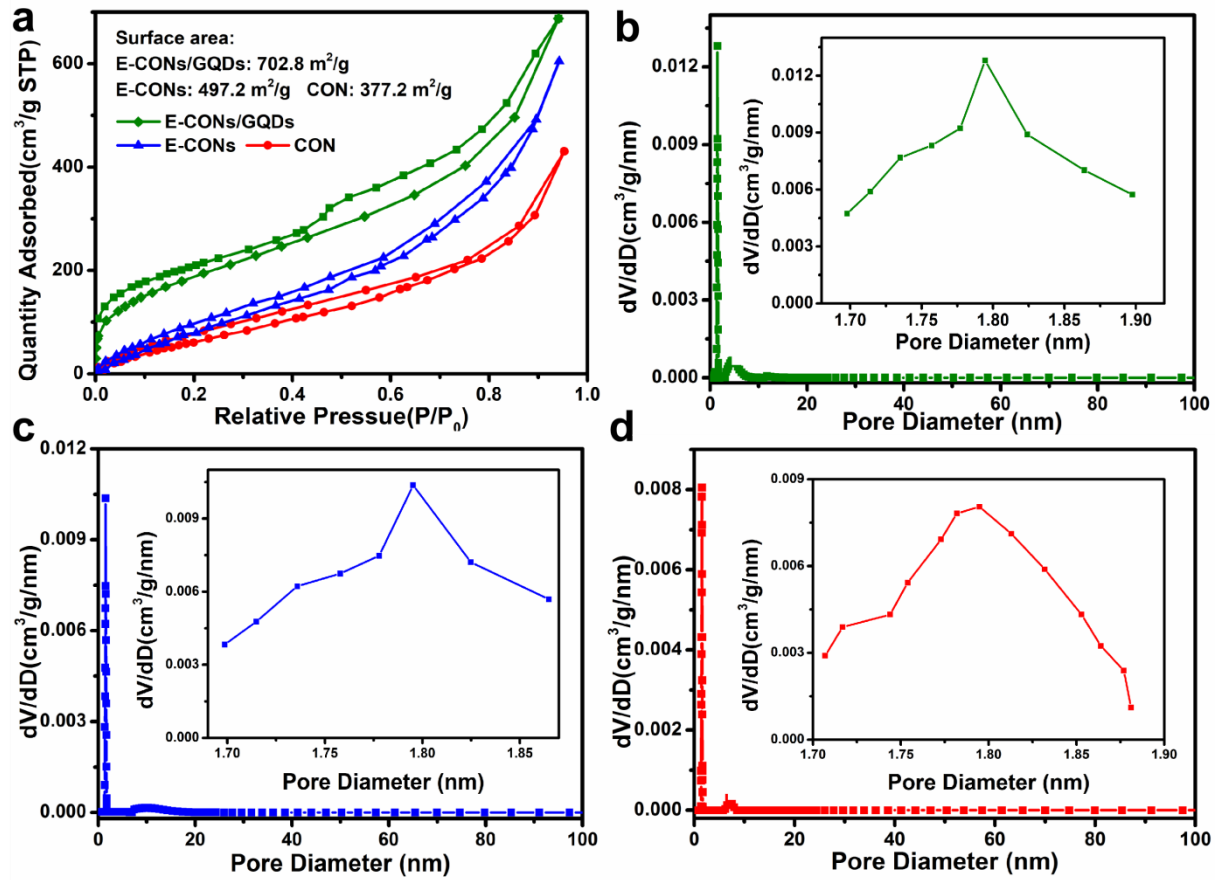


Fig. S5 BET results for E-CONs/GQDs and the control samples. a) N_2 adsorption/ desorption isothermal curves of the E-CONs/GQDs, E-CONs, and CON. The pore size distribution of b) E-CONs/GQDs, c) E-CONs and d) CON.

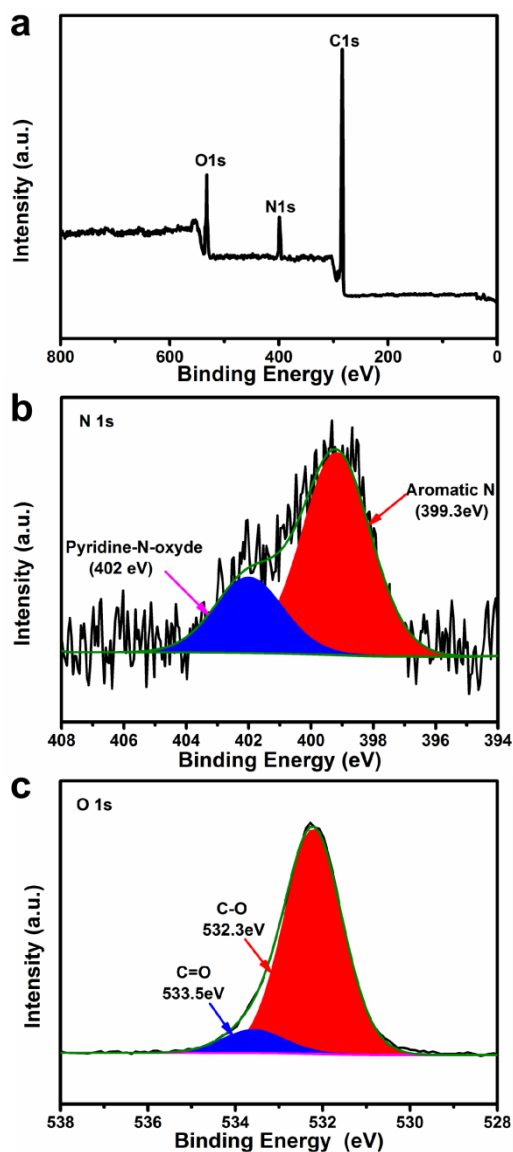


Fig. S6 XPS spectrum of as-prepared E-CONs/GQDs. a) Survey spectrum. High- resolution spectra of b) N1s, and c) O1s.

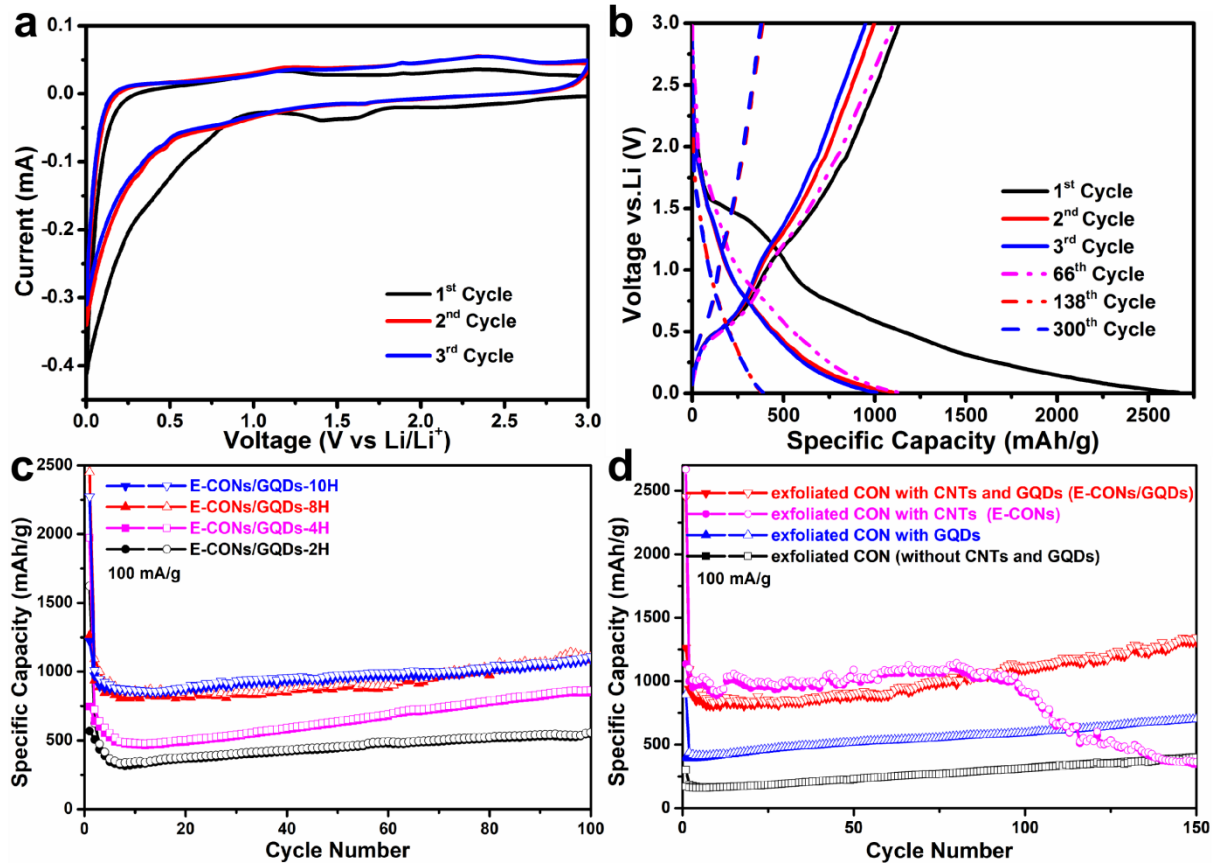


Fig. S7 Electrochemical performance of the control samples. **a)** Cyclic voltammograms curves and **b)** the discharge (lithium insertion) and charge (lithium extraction) curves of the E-CONs for the 1st, 2nd, 3rd, 66th, 138th, and 300th cycles at 0.1 A/g. The corresponding discharge/charge capacities are detected to be 2668/1136, 1101/999, 1010/950, 1128/1105, 383/376, 388/377 mAh/g, respectively. **c)** Cycling performances of the E-CONs/GQDs with different stripping times at 0.1 A/g. For the E-CONs/GQDs-2H, E-CONs/GQDs-4H, E-CONs/GQDs-8H, and E-CONs/GQDs-10H anodes, initial discharge/charge capacities are discovered to be 1623/568, 1973/746, 2452/1263, and 2272/1224 mAh/g, respectively. The reversible capacities of 546, 849, 1085, and 1091 mAh/g for E-CONs/GQDs-2H, E-CONs/GQDs-4H, E-CONs/GQDs-8H, and E-CONs/GQDs-10H anodes can be realized after 100 cycles, respectively. We can see that the electrochemical performance of the composite electrode material is significantly improved as the stripping time increases. However, the electrochemical performance improvement of E-CONs/GQDs-10H and E-CONs/GQDs-8H (named as: E-CONs/GQDs) is not very obvious. **d)** Cycling performances of the E-CONs/GQDs (exfoliated CON with CNTs and GQDs), E-CONs(exfoliated CON with CNTs), and exfoliated CON with GQDs, and exfoliated CON (without CNTs and GQDs) at 0.1 A/g. For the E-CONs/GQDs, E-CONs, exfoliated CON with GQDs, and exfoliated CON (without CNTs and GQDs) anodes, initial discharge/charge capacities are discovered to be 2452/1263, 2668/1136, 895/397, and 301/171 mAh/g, respectively. The reversible capacity of 1309, 347, 701 and 396 mAh/g for the E-CONs/GQDs, E-CONs, exfoliated CON with GQDs, and exfoliated CON (without CNTs and GQDs) can be realized after 150 cycles, respectively. These values are substantially smaller than the main products of E-CONs/GQDs.

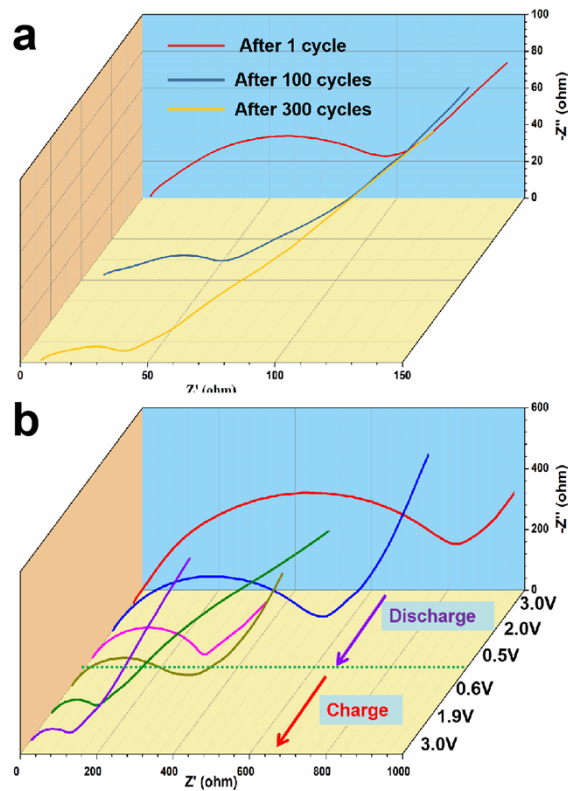


Fig. S8 Nyquist plots and Structural evolution characterizations of E-CONs/GQDs. a) Nyquist plots for E-CONs/GQDs after 1, 100 and 300 cycles. b) *In-situ* Nyquist plots recorded of the E-CONs/GQDs anode during the first discharge-charge cycle.

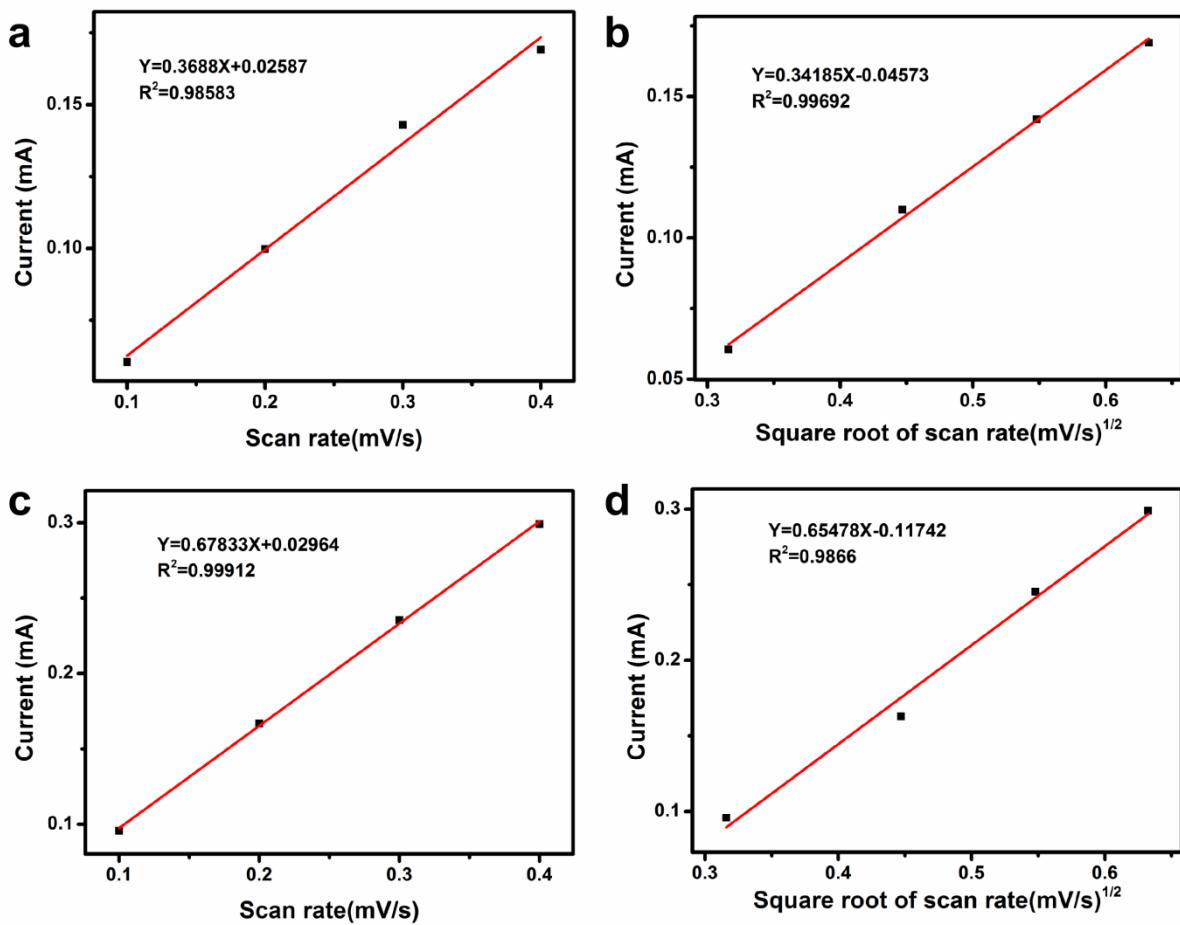


Fig. S9 The linear fit of the peak current for CV curves of different scan rates vs. the scan rate or the square root of scan rate. a,b) E-CONs/GQDs after 1 cycle and c,d) the E-CONs/GQDs after 300 cycles.

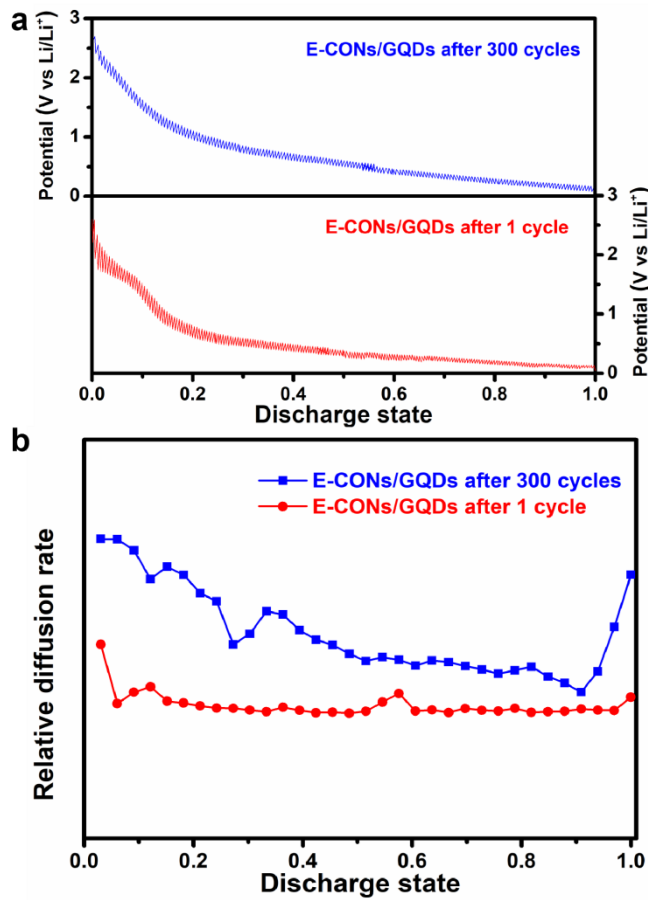


Fig. S10 GITT results for E-CONs/GQDs. a) Voltage-composition profile obtained for a Li/E-CONs-GQDs cell discharged to 0.005 V after 1 and 300 cycles in a GITT mode using an intermittent current rate of 100 mA/g and periodic interruptions whose length was determined by a voltage change of less than 1 mV per hour. b) The calculated Li chemical diffusion coefficients as a function of stoichiometry from the GITT results.

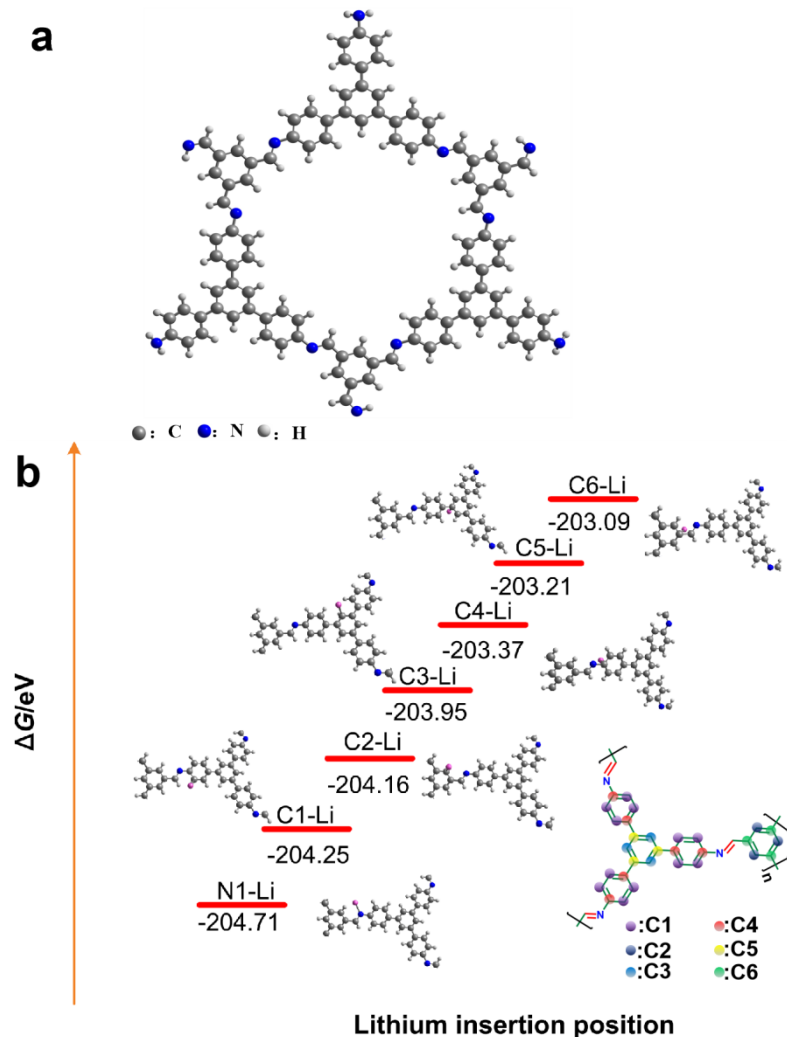


Fig. S11 The DFT results of CON monomer. a) The Geometry of three CON monomers. b) The calculated lithium insertion position. $\Delta G = E_{\text{Li-CON}} - E_{\text{CON}}$. N and C1 to C6 also correspond to the Li-insertion step.

Table S1. Elemental analysis results of E-CONs/GQDs, E-CONs, and bulk CON.

Samples	E-CONs/GQDs	E-CONs	Bulk CON
N (wt. %)	3.93	4.91	4.85
C (wt. %)	87.51	91.57	91.63
H (wt. %)	2.38	3.07	3.05

Table S2. The calculated Gibbs free energies for lithiation processes

Species	CON	CON-3Li	CON-15Li
G	-1622.5773	-1645.6007	-1737.8363
Reaction Processes		$\text{CON} + 3\text{Li}^+ + 3e^- \rightarrow \text{CON-3Li}$	$\text{CON-3Li} + 12\text{Li}^+ + 12e^- \rightarrow \text{CON-15Li}$
$\Delta G/\text{eV}$		-15.01	-63.90
$\Delta G_t/\text{eV}$			-78.91
Species	CON-18Li	CON-21Li	CON-27Li
G	-1761.0974	-1783.9284	-1830.2191
Reaction Processes	$\text{CON-15Li} + 3\text{Li}^+ + 3e^- \rightarrow \text{CON-18Li}$	$\text{CON-18Li} + 3\text{Li}^+ + 3e^- \rightarrow \text{CON-21Li}$	$\text{CON-21Li} + 6\text{Li}^+ + 6e^- \rightarrow \text{CON-27Li}$
$\Delta G/\text{eV}$	-21.48	-9.77	-36.65
$\Delta G_t/\text{eV}$	-100.38	-110.16	146.81
Species	CON-30Li	CON-33Li	
G	-1853.3609	-1876.5544	
Reaction Processes	$\text{CON-27Li} + 3\text{Li}^+ + 3e^- \rightarrow \text{CON-30Li}$	$\text{CON-30Li} + 3\text{Li}^+ + 3e^- \rightarrow \text{CON-33Li}$	
$\Delta G/\text{eV}$	-18.23	-19.64	
$\Delta G_t/\text{eV}$	-165.04	-184.68	

$G_{\text{Li}} = -7.4906$. ΔG_t corresponds to the total reaction of Gibbs free energy.

Table S3. The calculated Gibbs free energies of different Li-inserted position

Species	CON	N-Li	C1-Li	C2-Li	C3-Li
G	-1622.5773	-1630.1001	-1630.0834	-1630.0799	-1630.0723
		-7.5228	-7.5061	-7.5026	-7.4950
ΔG (eV)		(-204.71)	(-204.25)	(-204.16)	(-203.95)
Species	C4-Li	C5-Li	C6-Li		
G	-1630.0510	-1630.0452	-1630.0409		
	-7.4736	-7.4679	-7.4636		
ΔG (eV)	(-203.37)	(-203.21)	(-203.09)		

$\Delta G = E_{\text{Li-CON}} - E_{\text{CON}}$. N and C1 to C6 are also corresponding to the Li-insertion step.

Table S4. Electrochemical properties comparison between E-CONs/GQDs of this work and previous related electrodes by other researchers. (IRC: initial reversible capacity, mAh/g; RRC: retained reversible capacity, mAh/g; CN: cycle number; V: voltage, V; CD: current density, A/g). The capacity in the bracket of this work is the capacity contribution based on the E-CONs.

Composite	Li-storage active site	IRC	RRC/CN	Test condition (V, CD)	References
E-CONs/GQDs	C=N, aromatic C	1263	1386 (1687) /300	0.005-3,0.1	this work
DAPQ-COF50	C=O	146	111/3000	1.5-3.2,2	S1
TP-OH-COF	C=O	764.1	~800/100	0-3,0.1	S2
E-TFPB-COF/MnO ₂	C=N, aromatic C	1274	1359/300	0.005-3, 0.1	S3
E-TFPB-COF	C=N, aromatic C	1211	968/300	0.005-3, 0.1	S4
PPTODB	C=O	198	135/150	1.5-3.5,0.02	S4
PI-ECOF-1/rGO50	C=O	~160	~112/300	1.5-3.5,0.142	S5
COF@CNTs	C=N, aromatic C	383	1021/500	0.005-3,0.1	S6
IISERP-CON1	C=N, -OH	~750	~720/100	0.01-3,0.1	S7
N2-COF	C=N	689	600/500	0.05-3,1	S8
N3-COF	C=N	707	593/500	0.05-3,1	S8
TThPP-COF	C=O, C-NH, C-S	401	378/200	0.005-3,1	S9
Cz-COF1	C=N	~400	236/400	0.005-3,0.2	S10
Cz-COF2	C=N	~310	~150/400	0.005-3,0.2	S10
Tb-DANT-COF	C=O	127	80/200	1.5-4,0.2	S11

Tp-DANT-COF	C=O	79	~72/200	1.5-4,0.2	S11
DAAQ-ECOF	C=O	~90	104/1800	1.5-4,0.5	S12
PIBN-COF-Graphene	C=O	242	208/300	1.5-3.5,0.28	S13
D _{TP} -A _{NDI} -COF@CNTs	C=O	69	67/100	1.5-3.5,0.2	S14

References

- (S1) H. Gao, Q. Zhu, A. R. Neale, M. Bahri, X. Wang, H. Yang, L. Liu, R. Clowes, N. D. Browning, R. S. Sprick, M. A. Little, L. J. Hardwick and A. I. Cooper, Integrated Covalent Organic Framework/Carbon Nanotube Composite as Li-Ion Positive Electrode with Ultra-High Rate Performance, *Adv. Energy Mater.* 2021, **11**, 2101880.
- (S2) L. P. Zhai, G. J. Li, X. B. Yang, S. Park, D. D. Han, L. W. Mi, Y. J. Wang, Z. P. Li and S.-Y. Lee, 30 Li⁺-Accommodating Covalent Organic Frameworks as Ultralong Cyclable High-Capacity Li-Ion Battery Electrodes, *Adv. Funct. Mater.* 2021, **32**, 202108798.
- (S3) X. D. Chen, Y. S. Li, L. Wang, Y. Xu, A. M. Nie, Q. Q. Li, F. Wu, W. W. Sun, X. Zhang, R. Vajtai, P. M. Ajayan, L. Chen and Y. Wang, High-Lithium-Affinity Chemically Exfoliated 2D Covalent Organic Frameworks, *Adv. Mater.* 2019, **31**, 1901640.
- (S4) C. J. Yao, Z. Wu, J. Xie, F. Yu, W. Guo, Z. J. Xu, D. S. Li, S. Zhang and Q. Zhang, Two-Dimensional (2D) Covalent Organic Framework as Efficient Cathode for Binder-free Lithium-Ion Battery, *ChemSusChem* 2020, **13**, 2457-2463.
- (S5) Z. Wang, Y. Li, P. Liu, Q. Qi, F. Zhang, G. Lu, X. Zhao and X. Huang, Few layer covalent organic frameworks with graphene sheets as cathode materials for lithium-ion batteries, *Nanoscale* 2019, **11**, 5330-5335.
- (S6) Z. D. Lei, Q. S. Yang, Y. Xu, S. Y. Guo, W. W. Sun, H. Liu, L.-P. Lv, Y. Zhang, Y. Wang, Boosting lithium storage in covalent organic framework *via* activation of 14-electron redox chemistry, *Nat. Commun.* 2018, **9**, 576.
- (S7) S. Haldar, K. Roy, S. Nandi, D. Chakraborty, D. Puthusseri, Y. Gawli, S. Ogale and R. Vaidhyanathan, High and Reversible Lithium Ion Storage in Self-Exfoliated Triazole-Triformyl Phloroglucinol-Based Covalent Organic Nanosheets, *Adv. Energy Mater.* 2018, **8**, 1702170.
- (S8) L. Bai, Q. Gao and Y. Zhao, Two fully conjugated covalent organic frameworks as anode materials for lithium ion batteries, *J. Mater. Chem. A* 2016, **4**, 14106-14110.

-
- (S9) H. Yang, S. Zhang, L. Han, Z. Zhang, Z. Xue, J. Gao, Y. Li, C. Huang, Y. Yi, H. Liu and Y. Li, High Conductive Two-Dimensional Covalent Organic Framework for Lithium Storage with Large Capacity, *ACS Appl. Mater. Interfaces* 2016, **8**, 5366-5375.
- (S10) S. Feng, H. Xu, C. Zhang, Y. Chen, J. H. Zeng, D. L. Jiang and J.-X. Jiang, Bicarbazole-based redox-active covalent organic frameworks for ultrahigh-performance energy storage, *Chem. Commun.* 2017, **53**, 11334-11337.
- (S11) D. -H.Yang, Z.-Q. Yao, D. Wu, Y.-H. Zhang, Z. Zhou, X.-H. Bu, Structure-modulated crystalline covalent organic frameworks as high-rate cathodes for Li-ion batteries, *J. Mater. Chem. A* 2016, **4**, 18621-18627.
- (S12) S. Wang, Q. Wang, P. Shao, Y. Han, X. Gao, L. Ma, S. Yuan, X. Ma, J. Zhou, X. Feng and B. Wang, Exfoliation of Covalent Organic Frameworks into Few-Layer Redox-Active Nanosheets as Cathode Materials for Lithium-Ion Batteries, *J. Am. Chem. Soc.* 2017, **139**, 4258.
- (S13) Z. Q. Luo, L. J. Liu, J. X. Ning, K. X. Lei, Y. Lu, F. J. Li and J. Chen, A Microporous Covalent-Organic Framework with Abundant Accessible Carbonyl Groups for Lithium-Ion Batteries, *Angew. Chem. Int. Ed.* 2018, **57**, 9443-9446.
- (S14) F. Xu, S. Jin, H. Zhong, D. Wu, X. Yang, X. Chen, H. Wei, R. Fu and D. Jiang, Electrochemically active, crystalline, mesoporous covalent organic frameworks on carbon nanotubes for synergistic lithium-ion battery energy storage, *Sci. Rep.* 2015, **5**, 8225.